SF2A 2014
J. Ballet, F. Bournaud, F. Martins, R. Monier and C. Reylé (eds)

PDBI HIGH-RESOLUTION HIGH-SENSITIVITY IMAGING OF A STRONGLY LENSED SUBMILLIMETER SOURCE AT Z=5.24

F. Boone[1], F. Combes[2], M. Krips[3], J. Richard[4], T. Rawle[5], E. Egami[6], J.-P. Kneib[7], D. Schaerer[1,8], M. Dessauges-Zavadsky[8], R. Pello[1], B. Clément[4] and HLS team

Abstract. We have obtained Plateau de Bure Interferometer observations of HLSJ091828.6+514223 (z=5.24) at six different frequencies to cover the CO(6-5), CO(7-6), CI, H_20_p(2,0,2-1,1,1), [NII] and [CII] lines. The high resolution and high sensitivity of these multi-configuration observations allow us to detect the various line velocity components as well as the continuum and to resolve spatially their emission. This wealth of information is used to tackle the problem of lens and source modeling. A methodology is implemented to produce image plane maps, optimize the lens model, and finally inverse the PdBI data in the source plane. The image plane and source plane maps are constructed by fitting directly the pixels to the PdBI visibilities with the non-negative least square method. The preliminary results thus obtained are presented.

Keywords: high-redshift, gravitational lensing, submillimeter galaxies, molecular gas, dust emission

1 Introduction

HLSJ091828.6+514223 was discovered in the *Herschel* Lensing Survey (HLS, Egami et al. 2010) with an exceptionally bright flux of ∼200 mJy at 500μm. It is located behind the lensing galaxy cluster Abell 773 (z=0.22) and is further magnified by a z=0.63 galaxy. IRAM-30m with the EMIR backend allowed us to determine the redshift of the source at z=5.243 and to detect the CO(7-6), CO(6-5), CO(5-4), C I($^3P_2$–$^3P_1$) H_2O_p(2,0,2-1,1,1) and [NII]205μm lines (Combes et al. 2012). The CO(2-1) line was also detected at the EVLA.

We then simultaneously observed this bright northern submillimeter source at SMA and Plateau de Bure Interferometer (PdBI) to resolve the emission and detect the [CII] line. A deep analysis of the SMA data with a discussion of the various velocity components and PDR modeling is reported by Rawle et al. (2014).

Here we report on the high-resolution and high-sensitivity PdBI observations. We describe the method implemented to obtain a reliable lens model and to invert (or delens) the data.

2 Observations

From 2012 to 2014 we have obtained a total of 12 tracks with the 6 antennas of the Plateau de Bure Interferometer (PdBI) connected to the WIDEX correlator providing 3.6 GHz bandwidth. We observed at six different frequencies to cover the CO(6-5), CO(7-6), CI, H_20_p(2,0,2-1,1,1), [NII] and [CII] lines. The observations are summarized in the Table 1. The angular resolutions obtained are all below 1″ and reach 0.3″ at 304 GHz.

3 Imaging with the non negative least squares method

Because the emission detected with PdBI at all frequencies is compact (<5″ in diameter) and the signal-to-noise ratio is high, it is possible to solve the imaging problem with a least squares method. The flux of each pixel of

[1] IRAP, CNRS OMP-UPS, 14, avenue Edouard Belin 31400 Toulouse
[2] LERMA, Observatoire de Paris, 61 avenue de l'Observatoire, 75014 Paris, France
[3] IRAM, 300 rue de la Piscine, Domaine Universitaire, 38406 Saint Martin d'Hres, France
[4] Centre de Recherche Astrophysique de Lyon, Université Lyon 1, 9 Avenue Charles André, F-69561 Saint Genis Laval, France
[5] European Space Astronomy Centre (ESAC)/ESA, Villanueva de la Cañada, E-28691 Madrid, Spain
[6] Steward Observatory, University of Arizona, 933 North Cherry Avenue, Tucson, AZ 85721, USA
[7] Laboratoire d'astrophysique, Ecole Polytechnique Fédérale de Lausanne, Observatoire de Sauverny, 1290 Versoix, Switzerland
[8] Observatoire de Genève, Université de Genève, 50 Ch. des Maillettes, 1290 Versoix, Switzerland

Table 1. PdBI Observations of HLSJ091828.6+514223.

Freq [GHz]	line	config	beam [″]	noise [mJy] in 20 MHz channels
111	CO(6-5)	A	0.8×0.7	0.57
129	CO(7-6)+CI	ABD	0.9×0.7	0.49
158	H_2O_p(2,0,2-1,1,1)	AC	0.7×0.6	0.61
218	–	A	0.48×0.31	1.46
234	[NII]	ABCD	0.46×0.46	0.72
304	[CII]	A	0.31×0.27	2.68

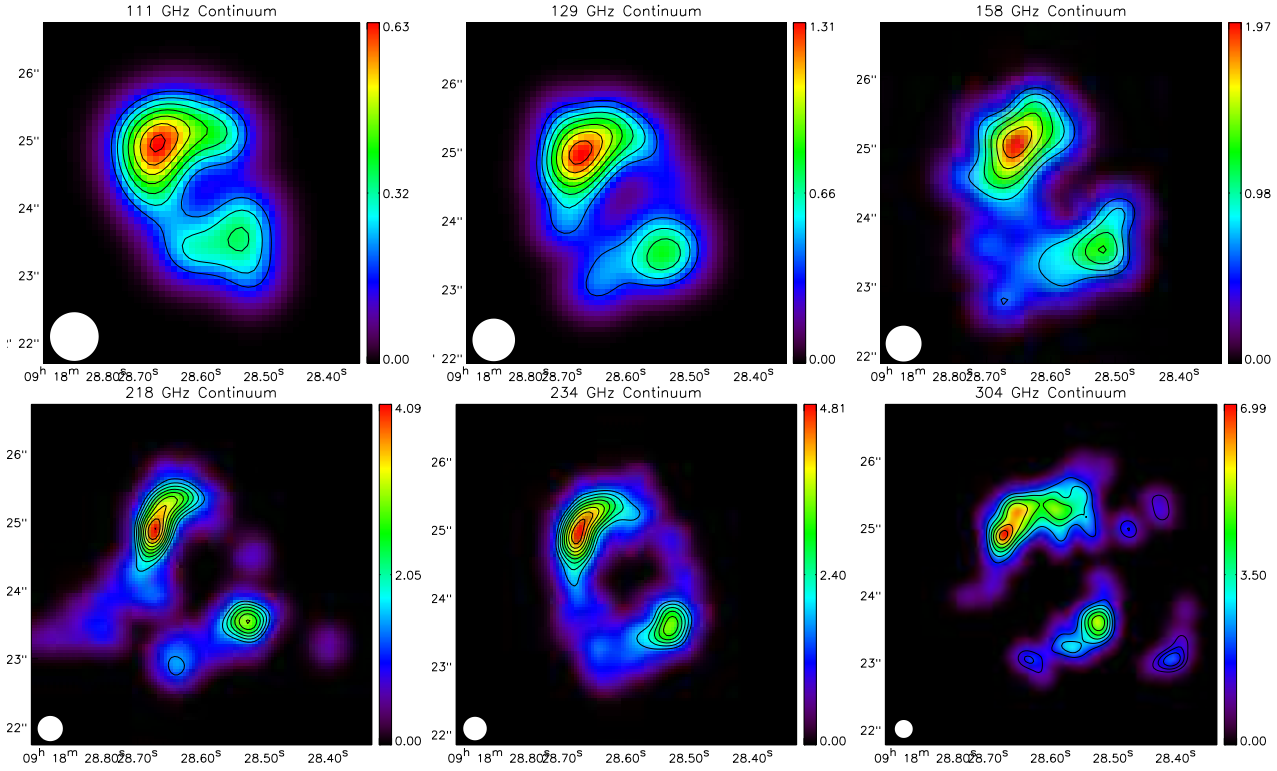

Fig. 1. PdBI continuum maps (2.5″ in size) obtained with the NNLS method. From left to right and from top to bottom the frequencies are 111, 129, 158, 218, 234 and 304 GHz. In each frame the white circle represents the resolution.

the region of interest in the image (sky) plane is considered as a free parameter, $s_i > 0$. The pixel values are the solution to the matrix equation:

$$V_i = \sum_{j}^{N_{\rm pix}} \mathrm{s}_j \times F_{ij}, \tag{3.1}$$

where, V_i are the complex visibilities measured at the coordinates (u_i, v_i) in the Fourier plane, $N_{\rm pix}$ is the number of pixels in the image plane and $F_{ij} = \mathcal{F}_j(u_i, v_i)$, where $\mathcal{F}_j(u, v)$ is the Fourier transform ($\mathscr{F}\{\}$) of a map in which $s_k = 0\ \forall k \neq j$ and $s_j = 1$, i.e.,

$$\mathcal{F}_j(u,v) = \mathscr{F}\{\delta(x - x_j, y - y_j)\} = \cos(2\pi(u\frac{x_j}{\lambda} + v\frac{y_j}{\lambda})) + i\sin(2\pi(u\frac{x_j}{\lambda} + v\frac{y_j}{\lambda})), \tag{3.2}$$

where (x_j, y_j) are the coordinates of the $j^{\rm th}$ pixel. We solve Eq. 3.1 with the non-negative least square method (Lawson & Hanson 1974) using pixels of size $dx = 0.5 \times$ BFWHM (beam full width at half maximum) in a circular region of radius $R = 2.5''$. The six maps thus obtained for the continuum are shown in Fig. 1, and the maps obtained for the four velocity components of the [CII] lines are shown in Fig. 2. By construction

these maps have no negative values as opposed to those obtained with the CLEAN method (due to negative residuals).

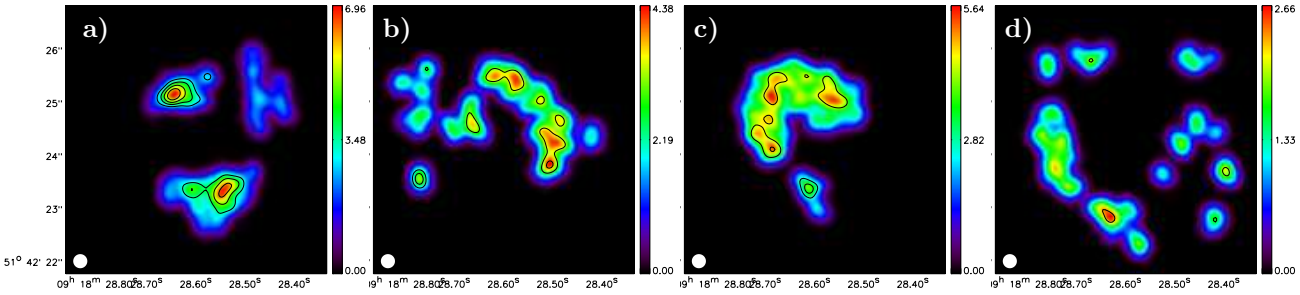

Fig. 2. PdBI maps of the four [CII] line velocity components obtained with the NNLS method. From left to right the integrated velocity intervals in km/s are [-30,420] (a), [-320, -30] (b), [-600,-320] (c) and [-1000, -600] (d).

4 Lens modeling

Modeling this lens is not straightforward because the source seems to be extended in the continuum at all wavelengths at which it is detected as well as in all the line velocity components. It is not possible to fit the lens parameters to accurate optical observations of a background point source as usually done for lensed quasars (e.g., Anh et al. 2013). This leads to degeneracies between source and lens parameters. The most compact images obtained in continuum at 304 GHz resemble a double system (Fig. 1) and can therefore be used to constrain the lens along one direction only. In addition, the various velocity components suggest that we are dealing with a complex source possibly composed of interacting galaxies and/or outflows/inflows (Rawle et al. 2014).

However, the lensing cluster A773 at $z = 0.22$ was already modeled by Richard et al. (2010) based on many multiple arc systems and the main lensing galaxy at $z = 0.63$ was detected with Subaru with no obvious companions (Combes et al. 2012) . We can therefore fix the cluster model to the one found by Richard et al. (2010) and add a single halo component for the additional lensing galaxy. We have therefore 5 free parameters: the galaxy center coordinates, its mass, ellipticity and position angle.

To optimize the lensing galaxy parameters we select intensity peaks in the NNLS maps of the continuum and the line components with high S/N. We use the LENSTOOL software (Kneib et al. 1996; Jullo et al. 2007) to take all these constraints into account assuming the peaks of a given velocity component are the multiple images of a single source. Although this assumption may not be valid for all the peaks (because the source is extended), by minimizing the number of sources the software is able to find the optimal solution.

5 Delensing PdBI data

Once a reliable lens model is obtained it is possible to delens the interferometric data and thus obtain directly source plane maps by using the same method as for image plane maps (Section 3). Indeed, Eq. 3.1 still applies with the definition of $\mathcal{F}_j(u, v)$ (Eq. 3.2) replaced by:

$$\mathcal{F}_j(u, v) = \mathscr{F}\{\mathscr{L}\{\mathcal{G}(x - x_j, y - y_j)\}\}, \tag{5.1}$$

where $\mathscr{L}$ represents the lensing operator, and where the δ functions representing the pixels have been replaced by Gaussian functions $\mathcal{G}$ to prevent discontinuities close to the caustic lines. To fully sample the source plane the Gaussian functions are taken circular with a FWHM equal to twice their separation.

We performed this lens inversion by applying the NNLS method to the PdBI data and we thus obtained a total of 30 source maps (6 continuum and 4 components for each of the 6 lines). For illustration we show the source maps obtained for the 304 GHz continuum and for one of the [CII] components together with the corresponding image maps in Fig.3. In Fig.4 we show the 4 velocity components of the [CII] line overlaid on the 304 GHz continuum. The continuum peak could be a galaxy nucleus surrounded by a rotating disk (red and blue contours). A complete interpretation of the various components will be discussed in a forthcoming paper.

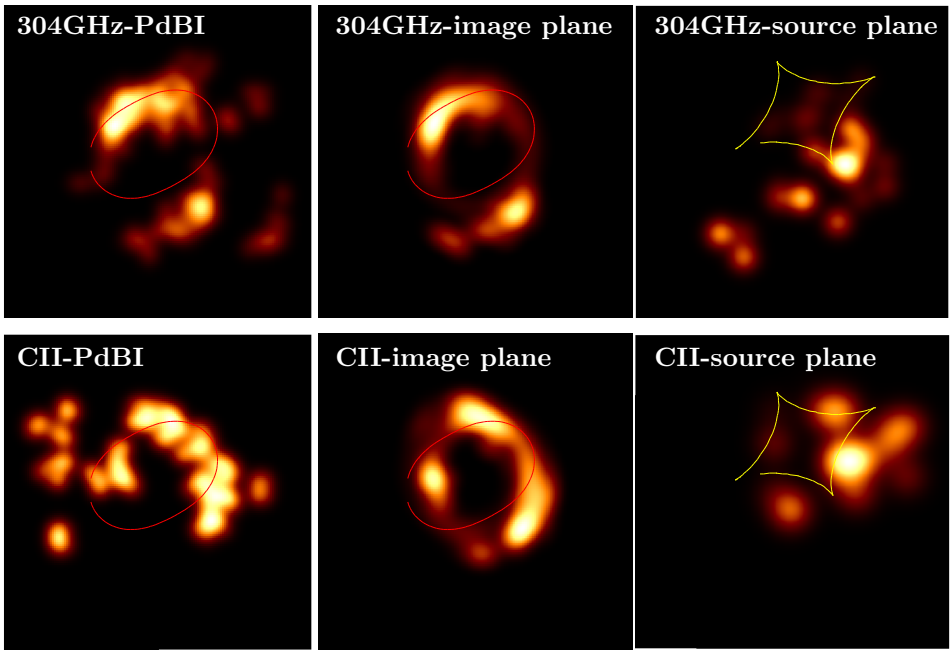

Fig. 3. The delensed source maps obtained for the 304 GHz and the [CII] line in the [-320, -30] km/s velocity interval are shown in the right-hand side frames. The corresponding image plane maps are shown in the middle frames and can be compared to the image plane maps obtained directly from the PdBI data shown on the left-hand side (same as in Figs. 1 and 2).

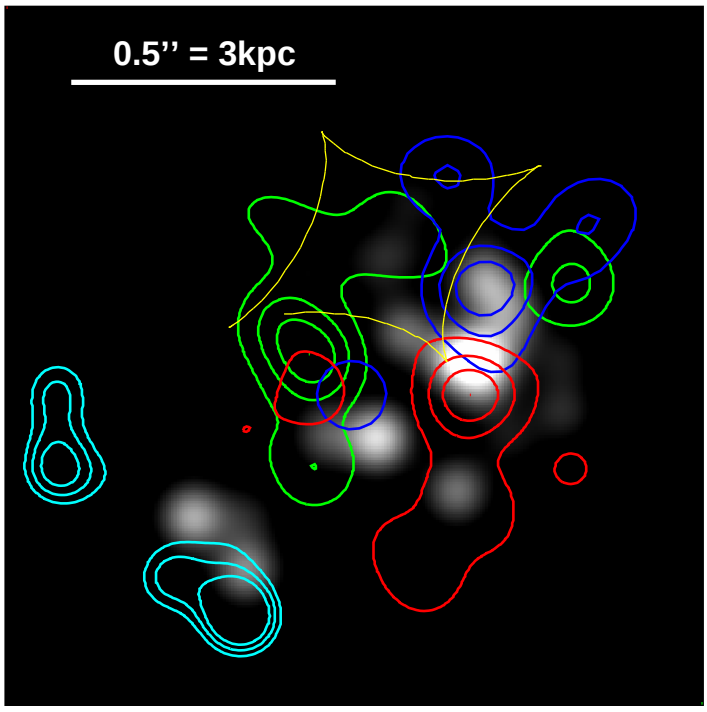

Fig. 4. Source plane delensed maps. The grey scale intensity map shows the 304 GHz continuum emission, the red, blue, green and cyan contours represent the [CII] line emission in the velocity intervals [-30,420], [-320, -30], [-600,-320] and [-1000, -600] km/s, respectively (see Fig. 2). The yellow line shows the caustic curve from the best lens model.

6 Conclusions

We have obtained a unique set of observations of HLSJ091828.6+514223 with PdBI. We developed methods and tools to allow their interpretation in the source plane. This will be the subject of a forthcoming paper.

We are very grateful to the IRAM staff for their kind help with the observations. We thank the Action Specifique ALMA of the CNRS for its support.

References

Anh, P. T., Boone, F., Hoai, D. T., et al. 2013, A&A, 552, L12
Combes, F., Rex, M., Rawle, T. D., et al. 2012, A&A, 538, L4
Egami, E., Rex, M., Rawle, T. D., et al. 2010, A&A, 518, L12
Jullo, E., Kneib, J.-P., Limousin, M., et al. 2007, New Journal of Physics, 9, 447
Kneib, J.-P., Ellis, R. S., Smail, I., Couch, W. J., & Sharples, R. M. 1996, ApJ, 471, 643
Lawson, C. L. & Hanson, R. J. 1974, Solving least squares problems
Rawle, T. D., Egami, E., Bussmann, R. S., et al. 2014, ApJ, 783, 59
Richard, J., Smith, G. P., Kneib, J.-P., et al. 2010, MNRAS, 404, 325